Transient heat exchanges under fast Reactivity-Initiated Accident

J-M Labit, N Marie, O Clamens, E Merle

Transient heat exchanges under fast Reactivity-Initiated Accident

J-M. Labit[1], N. Marie[1], O. Clamens[1] and E. Merle[2]
[1]CEA, DEN, DER
F-13108 Saint Paul-Lez-Durance, France

[2]CNRS-IN2P3-LPSC/Grenoble INP/UGA
53 Rue des Martyrs, 38026 Grenoble Cedex, France

jean-marc.labit@cea.fr

August 11, 2022

Abstract

Heat exchanges during fast transient are very complex phenomena. Many studies have been led in this field, trying to quantify the heat exchanges between a heating wall, under fast increasing power, and a coolant. This kind of situation is encountered for instance during RIA (Reactivity-Initiated Accidents) in nuclear reactors, whose characteristics times of wall heat flux excursion can be as low as orders of 1 ms. The CABRI reactor, an experimental pulse reactor funded by the french Institute for Radiological protection and Nuclear Safety (IRSN) and operated by CEA at the Cadarache nuclear center (France), was build in order to study and thus to better understand RIA effects on nuclear fuels. Heat exchanges characterization is definitely one of major points to tackle in the understanding and modeling of such transients, involving single and two phase flows.
This paper broaches the question of single phase heat exchanges coefficients during fast transient power excursions in the CABRI reactor.
The single phase pure convection is the overlap of two main mechanisms: the advection (wall axial supply in upstream cold water) and the turbulent mixing inside the boundary layer. This latter phenomenon is due to vortices in boundary layers inducing radial mixing through the velocity boundary layer. In most cases involving turbulent flows, the turbulent mixing phenomenon is preponderant. To these mechanisms is added a pure conduction heat exchange mechanism through the thermal boundary layer. Convection and conduction overlap defining a conducto-convective heat transfer coefficient, improperly only called "convection" coefficient. This paper suggests a way to model this coefficient during a CABRI-RIA transient by a non-linear superposition of transient pure conduction and convection mechanisms. Two distinct transient phases are considered; the first one presenting a wall heat flux of exponential shape followed by the second one during which the wall heat flux remains constant. The potency of this analytical model, which is implementable into computational system tools, is demonstrated.

Keywords— Transient heat exchange coefficient, RIA, analytical

Nomenclature

Acronyms

CATHARE	Code for Analysis of THermalhydraulics during an Accident of Reactor and safety Evaluation
CEA	Commissariat à l'Energie Atomique et aux Energies Alternatives (french Atomic Agency)
FWHM	Full Width at Half-Maximum
IRSN	Institut de Radioprotection et de Sûreté nucléaire (Institute for Radiological protection and Nuclear Safety)

PWR	Pressurized Water Reactor
RIA	Reactivity Initiated Accident

Mathematical operators and variables

Δ	Laplacian
div	Divergence
$\overrightarrow{\text{grad}}$	Gradient
p	Laplace complex frequency

Physical variables

α	Thermal diffusion coefficient ($m^2.s^{-1}$)
ΔT_{sat}	Subcooling (K)
δ_p	Thermal boundary layer thickness defined from the wall heat flux (m)
δ_t	Thermal boundary layer real thickness (m)
η	Dynamic viscosity (Pa.s)
λ	Conductivity ($W.m^{-1}.K^{-1}$)
ν	Cinematic viscosity ($m^2.s^{-1}$)
ϕ	Heat flux ($W.m^{-2}$)
ρ	Density ($kg.m^{-3}$)
τ	Wall heat flux excursion period (s)
τ_{adv}	Advection characteristic time (s)
τ_{vor}	Vorticity characteristic time in the velocity boundary layer (s)
Bi	Biot number
c_p	Heat capacity ($J.kg^{-1}.K^{-1}$)
D_h	Hydraulic diameter (m)
Fo	Fourier number
h	Heat exchange coefficient ($W.m^{-2}.K^{-1}$)
Nu	Nusselt number
Pr	Prandtl number
Re	Reynolds number
T	Temperature (K)
v	Velocity ($m.s^{-1}$)

Subscripts

0	Initial
∞	Bulk
cond	Conduction
conv	Convection
w	Wall

1 Introduction

This analytical work is part of a broader effort leading to the improvement and validation of the multi-physics modeling of CABRI-RIA transients with the system simulation tool CATHARE2 [1]. The CABRI reactor is an experimental pulse pool-type research reactor, funded by IRSN and operated by CEA at the Cadarache nuclear center in France [2]. It is designed to experimentally simulate a sudden and quasi-instantaneous power excursion, known as a power transient, typical of a Reactivity-Initiated Accident. This type of accident must be considered in the safety analysis of all reactors (not only PWRs). CABRI constitutes one of the most efficient experimental tool

(like for instance, in the 60-70's, the Special Power Excursion Reactor Test program - former SPERT reactor- [3]) to collect high burn-up test rods data on such complex multi-physics transients. In the CABRI core, the Helium depressurization from the transient rods injects up to 4 $ of reactivity triggering the power excursion. Thus, power pulses can reach a maximal instantaneous power around 20 GW with a Full Width at Half-Maximum (FWHM) around 10 ms. As detailed below, this reactor can provide many kinds of power pulses by controlling the Helium depressurisation (FWHM between 9-90 ms and power peak between 1-21 GW).

CATHARE2 (Code for Analysis of Thermal Hydraulics during Accident of Reactor and Safety Evaluation) [1, 4] has been developed by four French partners: the Atomic Energy Commission CEA, the safety institute IRSN, the utility EDF and the vendor FRAMATOME. This highly verified and validated tool is intended, among other things, for safety analyses with best estimate calculations of thermal-hydraulics transients in PWRs for postulated accidents or other incidents; quantification of conservative margins. The description of thermal non-equilibrium inhomogeneous two-phase flow is based on a two-fluid approach and six-equation model, using mainly algebraic constitutive relations for the modelling of interfacial coupling, wall friction, and wall heat transfer processes. This tool is able to model any kind of experimental facility or PWR (western type or VVER), and is usable for other reactors (fusion reactor, RBMK, BWR, research reactor, SFR). Unfortunately, currently it is not adapted and thus validated for the simulation of very fast RIA transients such as CABRI transients [1]. The final challenge is thus to succeed in simulating various various multi-physics reactivity insertion (RI) transients performed in the CABRI reactor catching the governing multiphysic phenomena with this CATHARE2 tool. During CABRI-RIA transients, the power transient is generated with controlled opening of the fast valves so that the helium under pressure can escape. This results in a sudden increase in reactivity (since the neutrons are no more absorbed, the fission rate increases) and thus to a power peak (the pulse). This is immediately limited by neutron feedbacks, mainly Doppler feedback effect, then at a lower level, thermal-mechanical clad expansion and moderating (mainly liquid thermal-expansion) feedback effects. Finally, the core is completely shut down by the control rods drop. Thus, these transients embrace fast phenomena under thermal-hydraulics, thermal-mechanics and neutronics coupling. After having reviewed the current capabilities of the CATHARE2 tool in regard to the main influential phenomena occurring during such RI transients (established from a QPIRT [5]), main improvements have been achieved [6];

- notably the improvement of the neutronic point-kinetics method to handle 3D effects in the core,
- the coupled modeling of the transient rods circuit with the reactor core; the depressurisation of these transient rods that induces the reactivity insertion inside the core,
- the thermomechanical model describing the evolution of the gap between the pellet and the clad,
- the clad-to-coolant heat transfer.

This work on clad-to-coolant heat transfer is presented in this paper.

This paper raises the issue of single-phase transient heat exchanges during fast reactivity insertion transients. Nowadays, most correlations used for both single and two-phase flows in system of component thermal-hydraulics simulation tools are still issued from steady-state experiments: Dittus-Boelter, Colburn, Sieder-Tate, Thom, Rosenhow *etc.* This is the case in CATHARE2 [1], RELAP5 [7], ATHLET [8] and TRACE [9]. However, plotting such models (the steady-state dotted curve in fig. 1) and RI-related experimental data on the same map shows a huge difference: the heat fluxes and temperature ranges of each regime differ significantly between the power transient case and the steady-state case described in the literature.

That is why dedicated tools devoted to rod-fuel analysis under RIA present specific dedicated clad-to-coolant heat transfer models. Hence, in the RANNS tool [11], developed to analyze thermal and mechanical behaviors of a single fuel rod in RIA conditions, the cladding surface heat transfer model for water coolant conditions is based on the vaporization model proposed by Bessiron et al. [10] and a classical heat transfer coefficient approach. In single phase, the clad-to-coolant heat transfer coefficient is calculated by the Dittus-Boelter's correlation when the wall is below the saturation temperature and above by the Chen's correlation. The aforementioned model parameters were fitted to the clad temperature measurement data from RIA-simulation/experiments with low flow conditions [12, 13]. Moreover, the SCANAIR simulation tool is specifically designed for analyses of RIAs in CABRI REP-Na test program. It comprises three main modules, dealing with thermal-dynamics (including thermal-hydraulics in the coolant channel). The coolant is modelled as a single phase fluid. The solution of the mass and energy conservation equations provides the coolant temperature and flowrate. Heat exchanges between the coolant and the clad are modelled by use of heat transfer coefficients obtained for the successive boiling regimes taking into account that phenomena are significantly different from steady-state conditions [14, 15]. Efforts are currently done to couple SCANAIR with two-phase thermal-hydraulics models in order to improve simulations in BWR conditions [16]. The thermal-hydraulics models of these tools still have a large part of empiricism. There are few thermal-hydraulics

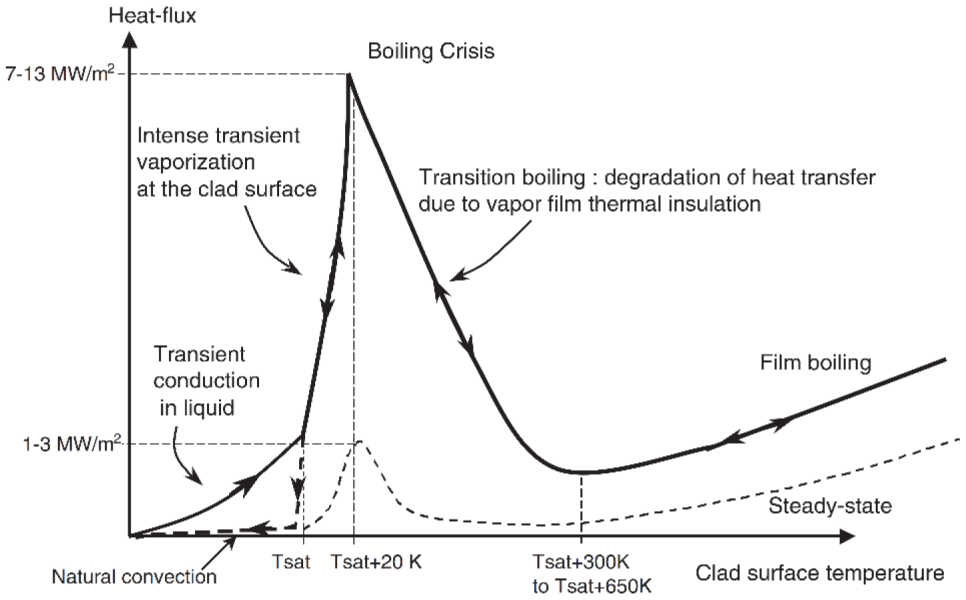

Figure 1: Schematic view of the experimental boiling curve in the fast RIA NSRR tests [10]

transient studies and a lack of understanding concerning transient boiling, even in simpler configurations. And due to the multiple phenomena involved in the reactor experiments, heat transfer coefficient values deduced from the current database could not be directly applied during RIA transient to any real plant. Thus, statistical analysis of numerical simulations obtained with a set of RIA fuel rod codes has been considered in the CSNI WGFS RIA fuel code benchmark [17] and showed that the scattering is large in the prediction of temperature transients.

The goal of the present analysis is to go beyond this statement by determining a physically based and analytical expression of the clad-to-coolant heat transfer in single-phase flow more than an adaptation by empirical fitting of classical steady-state models. Indeed, although heat transfers in convection regime is already much higher than in steady state (see figure 1), all the above-discussed simulation codes consider steady-state closure laws (Dittus-Boelter *etc.*). However this regime is of a major interest in the CABRI core.

To complete this work, we have considered most recent separate effect tests studies led under transient conditions in order to better understand these mechanisms, for single and two phase flows [18, 19]. These studies are the continuation of older works [20, 21, 22, 23]. They have also demonstrated that transient heat transfer coefficients can be much different from steady-state heat transfer coefficients. These studies, which postulate that RIA transient could be assimilated to heat flux exponential excursions, provide a lot of experimental results in the scope of single phase heat exchanges (also for transient boiling and critical heat flux).

However, these works are not complete to study the wall heat flux evolution during a CABRI RIA transient in its entirety. Indeed, during a reactivity test insertion in the CABRI reactor, the reactivity evolution is immediately limited by neutron feedbacks. Thus, the clad-to-coolant heat flux in the CABRI core (displayed on figure 2 for a heat exchange coefficient obtained with the Dittus-Boelter correlation) could only be assimilated to an exponential heat flux during the early beginning of the transient but no longer after. We will show that the duration of this exponential wall heat flux excursion is very small in comparison with the duration of the whole transient. Therefore, expressions of the heat exchange coefficient during the excursion given by these authors [18, 19] is not applicable for a complete CABRI-RIA transient. Moreover, even if some expressions exist for transient heat exchanges during the exponential excursion phase, their practical application in a calculation tool remains technically difficult: they require information from the end of the calculation in order to be applied, which is a non sense for their adaptation in a code. And thus, they have never, until now, be adapted in codes.

Therefore, the present paper proposes a new analytical expression for the clad-to-coolant heat exchange coefficient, improved from the studies of [18] and [20], enabling to be implemented in a system code like CATHARE2 and to simulate the whole CABRI-RIA transient and not the first exponential part only. Following the shape of the heat flux during a transient (cf. figure 2) in the CABRI reactor, a clad-to-coolant heat exchange coefficient for the whole transient has been developed considering the succession of phases: an early phase where the wall heat flux is assimilated to an exponential heat flux corresponding to the flux excursion (like in the previous studies) and second phase presenting a constant heat flux.

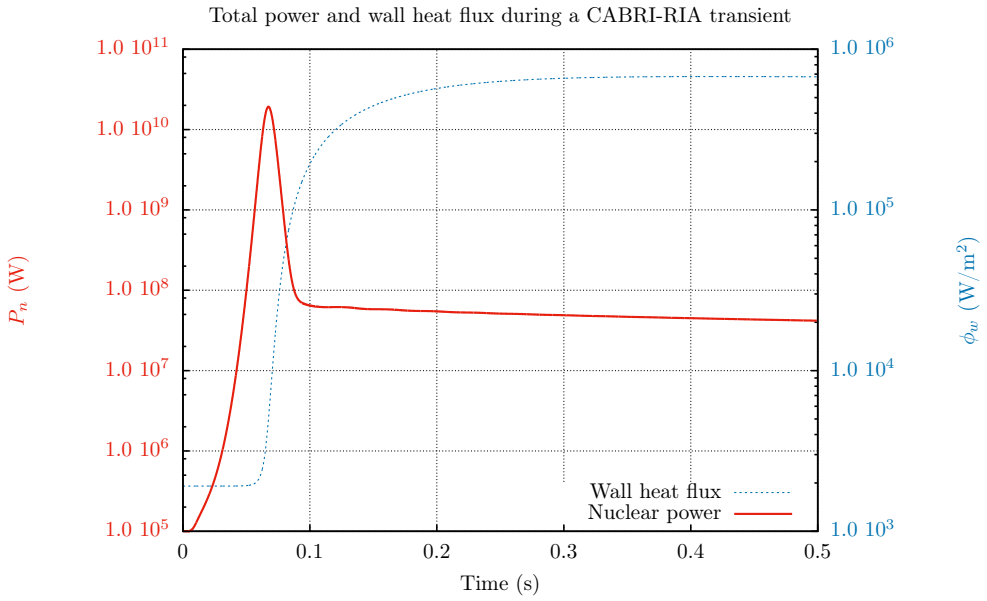

Figure 2: Example of core power and clad-to-coolant heat flux on one fuel rod during a CABRI-RIA transient

This paper first tackles the model for the early phases of the CABRI RIA transients. It presents an overview of the experimental studies of transient clad-to coolant heat exchanges under exponential heat flux that have been made in the MIT [18, 19], before detailing a new analytical work that has led to a new expression of the transient heat exchange coefficient in single-phase flow. This theoretical expression is then compared to the experimental results of MIT [19] for validation purpose. The second phase of the CABRI RIA transients is then modeled and linked to the exponential early phase. Finally, the paper deals with the implementation of this new model in CATHARE2 and the first impact studies. The achievement of the final goal, of being able to simulate the entirety of the transient heat transfer in CABRI-RIA test, is illustrated by the simulation of a complete CABRI fast transient including this new model.

2 An overview of experimental studies of transient exchanges

2.1 Pool heat exchanges under exponential heat flux

Before approaching convection effect on heat exchanges, some studies have been made in order to study heat transfers in a pure conductive way under an exponential heat flux.

Rosenthal [23] early noticed that the transient conduction in the water is governing the heat exchanges under transient conditions. Its experimental apparatus consisted in a ribbon immersed in a pool. The power of the ribbon increases exponentially with different excursion period τ. Sakuraï et al. [20, 21, 22] went further by measuring heat exchange coefficient and establishing the link between this coefficient and the excursion period, in an experiment very similar to Rosenthal's one. They suggested, based on transient conduction calculations, an asymptotic heat exchange coefficient for small excursion periods, varying as a function of $1/\sqrt{\tau}$.
The MIT's experiment presented in [18] consists in a wall heated with an exponential power source and exchanging energy with stagnant water. Its aim is to study both single and two phase heat exchanges between the heating wall and the water. The power source also delivers a thermal power of exponential shape like $e^{t/\tau}$ with different wall heat flux excursions period noted τ. From that experiment, Su et al. have deduced that the transient under exponential heat flux can be separated into two main steps. First, when the wall temperature increases, the thermal boundary layer grows. Then, in the second step of the thermal exchange, it comes a time at which this thermal boundary layer reaches a maximum thickness whereas the heat flux keeps increasing.

Su et al. [18] show that the wall temperature reaches an asymptotic behavior (*i.e.* when transient time tends to infinity, defined in [18] as $t > 3\tau$) proportional to the asymptotic heat flux during this second step. This implies that the heat exchange coefficient reaches a finite and non-zero asymptotic limit value depending on the excursion period τ. According to [18] this asymptotic value depends significantly on the excursion period τ but not on the

water subcooling because of the slow evolution of the value of the liquid water thermal diffusion coefficient with temperature.

2.2 Flow heat exchanges under exponential heat flux

Other studies were led in order to deal with the convection effect on heat exchanges during fast transients [19]. Experimental conditions are the same as in [18] and a cooling loop provides different Reynolds numbers and a manageable subcooling of the fluid in front of the wall. The objective is to measure the impact of subcooling and of the Reynolds number on the transient heat exchanges, driven by both pure transient conduction and convection. The single phase pure convection is the overlap of two main mechanisms: the advection (wall axial supply in upstream cold water) and the turbulent mixing in the boundary layer. This latter phenomenon is due to vortex in boundary layers inducing radial mixing through the velocity boundary layer. Su et al. [19] show that, in most cases involving turbulent flows, the turbulent mixing phenomenon is preponderant, because the vorticity time scale into the boundary layer τ_{vor} is smaller than the advection time scale τ_{adv}. To these mechanisms is added a pure conduction heat exchange mechanism through the thermal boundary layer. Convection and conduction overlap in order to give a conducto-convective heat transfer coefficient, generally only called "convection" coefficient.

The experimental results are presented in [19] with normalised heat transfer coefficient $\overline{h}$ as a function of the normalised period $\overline{\tau}$:

$$\begin{cases} \overline{h} = \dfrac{h_w(\tau, Re, \Delta T_{sat})}{h_{fc,exp}(Re, \Delta T_{sat})} & \text{(1a)} \\ \overline{\tau} = \dfrac{\tau}{\tau_{vor}} & \text{(1b)} \end{cases}$$

The vorticity time scale, which is involved in the definition of the normalised period, is given in [19] by $\tau_{vor} = D_h/(2v_\infty)$. This variable is surprisingly not dependent on the fluid properties but only on geometrical features and bulk velocity. $h_{fc,exp}(Re, \Delta T_{sat})$ is the heat exchange coefficient given by a steady-state forced convection given by the Sieder-Tate correlation. This correlation has been previously validated in steady-state on this experiment. And $h_w(\tau, Re, \Delta T_{sat})$ is the heat exchange coefficient issued obtained from measurements during the excursion period. The authors notice that all the experimental points of $\overline{h}$, defined in (1) , follow the same trend. This has led them to suggest the following correlation for $\overline{h}$ as a function of $\overline{\tau}$ with $n = 2$ [19]:

$$\overline{h} = \sqrt[n]{1 + \frac{1}{\sqrt[n]{\overline{\tau}}}} \tag{2}$$

One must notice that there seems to be a typing error in this expression. Indeed, when $\tau \to 0$, the theoretical trend of normalised heat exchange coefficient is in $1/\sqrt{Fo}$ with $Fo = \alpha\tau/D_h^2$ the asymptotic Fourier number. Thus when $\tau \to 0$, $\overline{h} \to 1/\sqrt{\overline{\tau}}$. Consequently, the correct expression should be:

$$\overline{h} = \sqrt[n]{1 + \frac{1}{\sqrt{\overline{\tau}}^n}} \tag{3}$$

Furthermore, it is worth underlying that the heat exchange coefficients could be only measured in the asymptotic regime in [18] and in [19] experiments (corresponding to the second physical step detailed in §2.1, when $t > 3\tau$). Thus, the step of establishment of the thermal boundary layer, when the heat exchange coefficient depends on both τ and t, is not covered by [18] and [19] heat transfer expression. It could be however significant for excursion heat fluxes presenting medium and high τ.

In the following, a theoretical expression of the heat exchange coefficient during and after the establishment of the thermal boundary layer will be derived based on the work of Su et al. [19] and compared to these experimental data. The heat exchange coefficient that will thus be time and period dependent. Moreover, the development of this heat transfer coefficient will no more be based on the overlap of conduction and convection characteristic times but the overlap of their corresponding heat transfer coefficients themselves. The vorticity time scale expression will be expressed in a more physical manner from fluid properties. This coefficient will be implemented in CATHARE2 tool for CABRI-RIA modeling. As heat conduction inside the fuel rods is already well modeled in CATHARE2, it results that transient conduction requires to be studied in water only.

3 Theoretical study of transient heat exchanges

The development of the theoretical expression of the heat exchange coefficient for the early phase (under exponential heat flux) is detailed in this section and its expression in the second phase is given in section 4.

3.1 Pure conduction

Situation analysis:
A fluid is in contact with a hot plane wall. It is assumed that the wall provides to the fluid a heat flux proportional to $e^{t/\tau}$. The fluid forms a semi-infinite medium and remains liquid. Main assumptions and initial and boundary conditions are presented in fig. 3. The aim is to derive analytical expression for the thermal boundary layer thickness

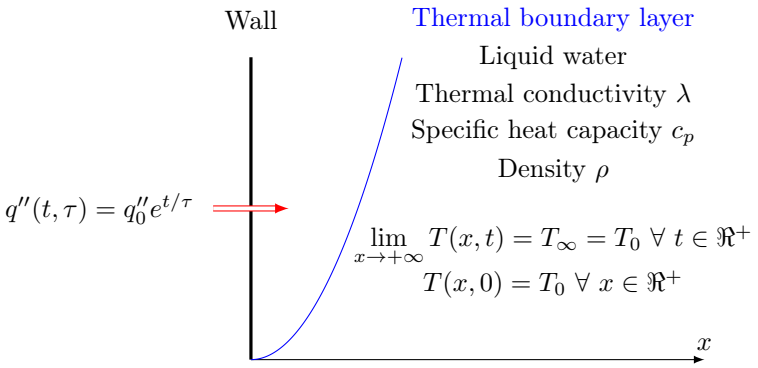

Figure 3: Theoretical situation

and for the heat exchange coefficient in pure conduction.

Resolution:
Heat conduction equation in the fluid is written as:

$$\rho c_p \frac{\mathrm{d}T}{\mathrm{d}t} + \mathrm{div}(-\lambda \overrightarrow{\mathrm{grad}}(T)) = 0 \tag{4}$$

Given that there is no convection in this situation and assuming no temperature variation along the wall, the temperature of the fluid only depends on x and t. We assume a constant conductivity. If $\theta = T - T_\infty$, we obtain :

$$\frac{\partial \theta}{\partial t} - \alpha \frac{\partial^2 \theta}{\partial x^2} = 0 \tag{5}$$

In order to solve this equation, the Laplace transform $\mathcal{L}$ of θ is used, that can be written Θ. Then :

$$\mathcal{L}\left(\frac{\partial \theta}{\partial t}\right) - \alpha \frac{\partial^2}{\partial x^2}\mathcal{L}(\theta) = 0 \tag{6}$$

With Laplace transform properties, we get $\mathcal{L}(\frac{\partial \theta}{\partial t}) = p\mathcal{L}(\theta) - \theta(x,0)$. Hence we obtain the differential equation:

$$p\Theta - \alpha \frac{\partial^2}{\partial x^2}\Theta = \theta(x,0) \tag{7}$$

We have $\theta(x,0) = 0$ (cf. fig. 3). A solution of the equation (7) is:

$$\Theta(x,p) = Ae^{-qx} + Be^{+qx} \tag{8}$$

Where $q = \sqrt{p/\alpha}$. The temperature is limited, according to the boundary condition in fig. 3. This implies that $B = 0$. A is determined thanks to the boundary condition on the wall:

$$-\lambda \left.\frac{\partial \theta}{\partial x}\right|_0 = q''_0 e^{t/\tau} \tag{9}$$

The Laplace transform of this condition gives:

$$-\lambda \left.\frac{\partial \Theta}{\partial x}\right|_0 = q_0'' \frac{1}{p - \frac{1}{\tau}} \tag{10}$$

And leads to:

$$\Theta(x,p) = \frac{q_0''}{\lambda q} \frac{1}{p - \frac{1}{\tau}} e^{-qx} \tag{11}$$

This expression can be inverted with inverse Laplace transform tables [24] and we obtain:

$$\theta(x,t) = \frac{q_0''}{\lambda} \frac{1}{2} e^{t/\tau} \sqrt{\alpha\tau} \left(e^{-x/\sqrt{\alpha\tau}} \text{erfc}\left(\frac{x}{2\sqrt{\alpha t}} - \sqrt{\frac{t}{\tau}} \right) - e^{+x/\sqrt{\alpha\tau}} \text{erfc}\left(\frac{x}{2\sqrt{\alpha t}} + \sqrt{\frac{t}{\tau}} \right) \right) \tag{12}$$

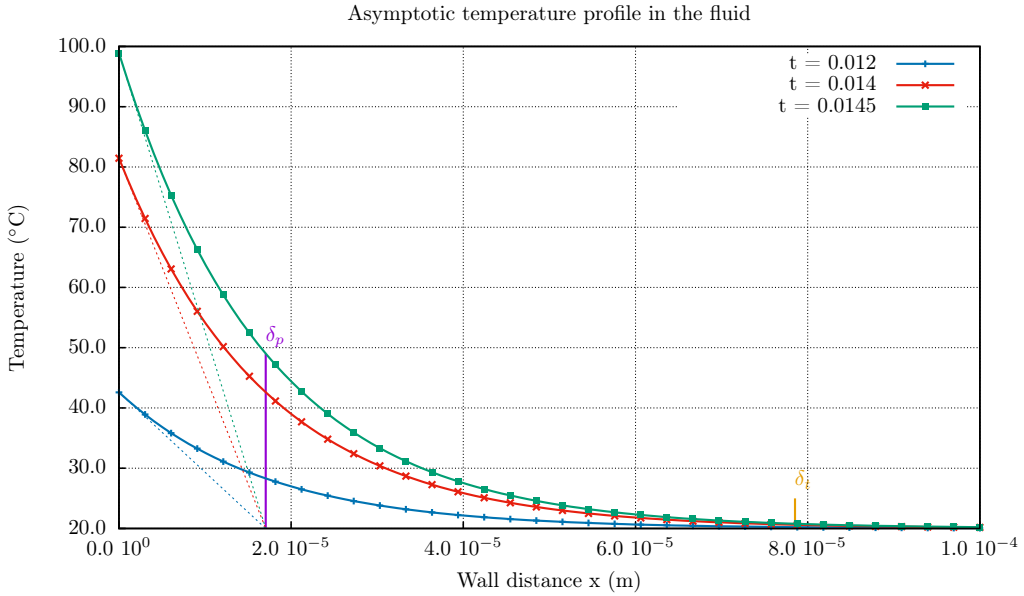

Figure 4: Solution of the equation (5) with $\tau = 2$ms

The fluid temperature evolution along the perpendicular distance to the wall is drawn in fig. 4 with $\tau = 2$ ms at different times in asymptotic conditions ($t > 3\tau$) for illustrative purpose.

Practical application:
We then have to determine the heat exchange coefficient h_{cond} as:

$$h_{cond}(T(0,t) - T_\infty) = -\lambda \left.\frac{\partial T}{\partial x}\right|_0 \tag{13}$$

After some steps, we obtain:

$$h_{cond} = \frac{\lambda}{\sqrt{\alpha\tau}\ \text{erf}(\sqrt{t/\tau})} \tag{14}$$

If δ_p, the thermal boundary layer thickness, is defined as :

$$-\lambda \left.\frac{\partial T}{\partial x}\right|_0 = -\lambda \frac{T_w - T_\infty}{\delta_p} \tag{15}$$

We obtain :

$$\delta_p = \sqrt{\alpha\tau} \text{erf}\left(\sqrt{\frac{t}{\tau}} \right) \tag{16}$$

The asymptotic value of δ_p (with $\text{erf}\left(\sqrt{t/\tau}\right) \approx 1$) is displayed in fig. 4. δ_p is not rigorously equal to the boundary layer thickness δ_t usually defined as $T(\delta_t, t) - T_\infty = 1\%(T(0,t) - T_\infty)$. With this definition, we find :

$$\lim_{t \to +\infty} \delta_t = 2\sqrt{\alpha\tau}\ln(10) \tag{17}$$

which is also displayed for illustration in fig. 4.

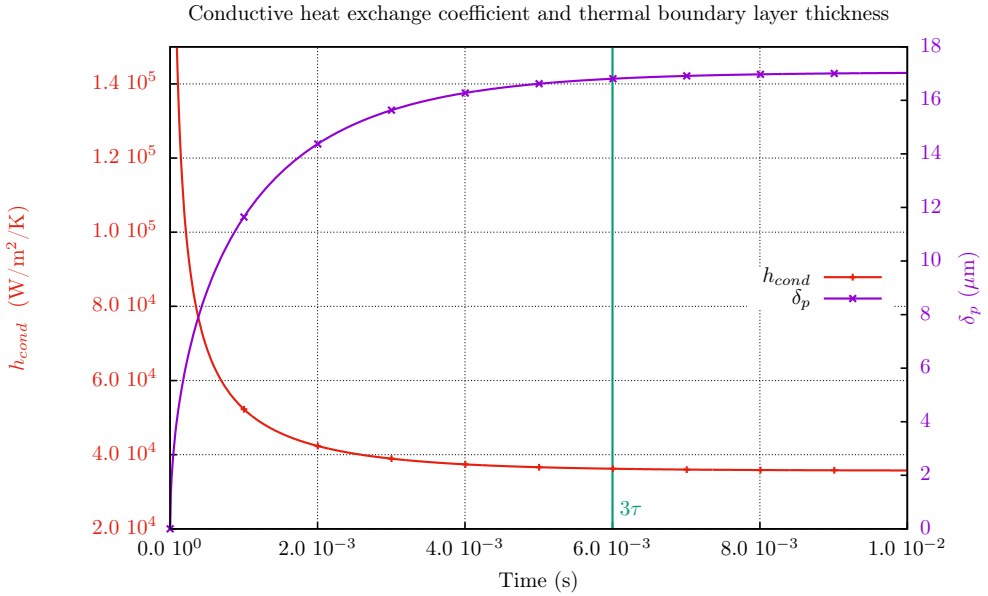

Figure 5: Conductive heat exchange coefficient with $\tau = 2$ ms

The difference between these two values is illustrated in fig. 4. We note that, in this studied asymptotic regime ($t > 3\tau$), the ratio of δ_t and δ_p remains constant and the thermal boundary layer thickness (δ_p) reaches a limit value as explained before and observed in experiments [19]. This observed physical behavior reinforces this development. An other point to raise is the fact that the thermal boundary layer thickness during the exponential excursion is much lower than the hydraulic diameter in a rod bundle. This "semi-infinite" approach is then valid.

The heat exchange coefficient and the thermal boundary layer thickness are drawn in fig. 5 for $\tau = 2$ ms and for water properties. As shown in this graph, the heat exchange coefficient due to pure conduction is very high (around 10^5 W/m^2/K) at the beginning of the transient and reach in asymptotic regime value as high as, around 4 10^4 W/m^2/K. As a comparison, the heat exchange coefficient due to convection is approximately 1.5 10^4 W/m^2/K in the CABRI reactor core, calculated with the standard Dittus-Boelter correlation. Thus conduction heat exchange type is not negligible compared to convection type. Moreover, the asymptotic regime appears clearly in fig. 5 after $t > 4$ ms (where $\tau = 2$ ms). The conductive heat exchange approaches its asymptotic value after 3τ.

3.2 Convective and conductive heat exchanges superposition

According to these previous analyses, the transient conduction should be taken into account in the total heat exchange coefficient under transient power insertion. We assume as in [19], that the radiative heat exchanges between the clad and the fluid are totally negligible and then will not be studied. The overlap of the conductive and convective heat exchange phenomena is *a priori* non-linear, given that the relative efficiency of conductive heat exchange in comparison with convective heat exchange is not constant with the period τ and time t. Thermal conductances can not be added as it would be in a parallel thermal resistances problem. The overlap of these phenomena depends on the competition between convection and conduction through the boundary layers. The ratio of velocity boundary layer and thermal boundary layer is driven by the Prandtl number.
These effects can then be superposed with a non-linear expression to derive a total heat exchange coefficient h.

$$h = \left(h_{conv}^n + h_{cond}^n\right)^{1/n} \tag{18}$$

h_{conv} can be deduced from steady-state forced convection correlations (Dittus-Boelter, Sieder-Tate, etc.). The overlap of these phenomena can be expressed following eq. (18) with one of these steady-state correlations if the

velocity boundary layer is established; *i.e.* in this case the convection is not transitory. This assumption is consistent with the CABRI case.
From eq. (18) and (14), we deduce:

$$h(t,\tau) = \left(1 + \left(\frac{\lambda}{\sqrt{\alpha\tau}\ \mathrm{erf}\left(\sqrt{t/\tau}\right) h_{conv}}\right)^n\right)^{1/n} h_{conv} \tag{19}$$

The error function $\mathrm{erf}(x)$ tends very fast to 1 when $x \to +\infty$ and thus, in asymptotic regime, a limit value is reached by the heat exchange coefficient h_{asym}:

$$h_{asym}(\tau) = \lim_{t\to+\infty} h(t,\tau) = \left(1 + \left(\frac{\lambda}{\sqrt{\alpha\tau} h_{conv}}\right)^n\right)^{1/n} h_{conv} \tag{20}$$

We have thus derived a time dependent clad-to-coolant heat coefficient and this asymptotic expression (for $t \to +\infty$) makes possible the determination of n in eq. (19). To achieve that, we have drawn in fig. 6, experimental results of [19] and the normalised asymptotic heat transfer coefficient ($h_{asym}(\tau)/h_{conv}$) as a function of the normalised excursion period $\overline{\tau}$ given in eq. (22):

$$\overline{h_{asym}}(\overline{\tau}) = \left(1 + \left(\frac{1}{\sqrt{\overline{\tau}}}\right)^n\right)^{1/n} \tag{21}$$

Where :

$$\begin{cases} \overline{\tau} = \dfrac{\tau}{\tau_{vor}} & \text{(22a)} \\ \tau_{vor} = \dfrac{\lambda^2}{\alpha h_{conv}^2} = \dfrac{\lambda\rho c_p}{h_{conv}^2} & \text{(22b)} \end{cases}$$

This normalised period depends on a vorticity time scale which, that time, depends on fluid properties and is expressed by equation (22)

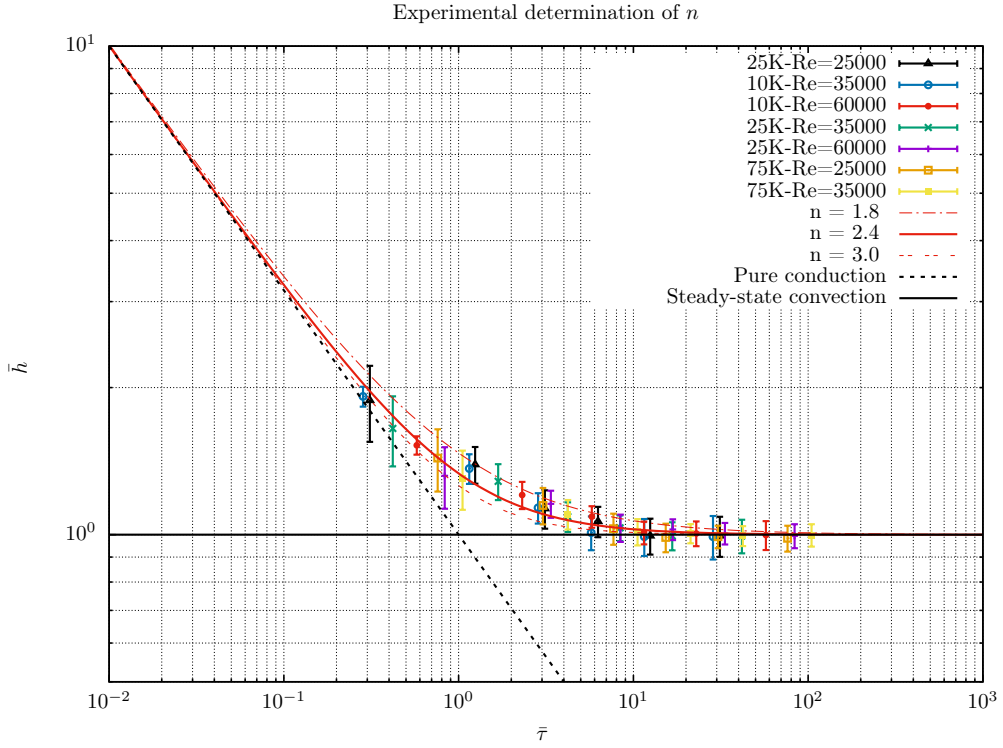

Figure 6: Determination of n with experimental results from [19]

The experimental data and their associated uncertainties of [19] have been plotted with the definition of this new expression of τ_{vor} in eq. (22) and not with the one given in [19] ($D_h/(2\ v_\infty)$) in order to have a normalised period consistent with our model of a total heat exchange coefficient. This vorticity time should logically depend on the thermal and cinematic properties of the fluid, contained in h_{conv} in eq. (22). fig. 6 shows that the heat transfer model agrees well with the experiments for $n = 2.4 \pm 0.6$.

The characterisation of the variable uncertainty range would enable to carry out uncertainty propagation studies with this developed RI version of CATHARE2 in near future.

The obtained global trend of the heat exchange coefficient is physically consistent: heat exchange coefficients in steady state convection are obtained for large normalised power excursion periods and heat exchange coefficients in pure conduction trend are obtained for small periods. Finally, we write:

$$h(t,\tau) = \left(1 + \left(\frac{\lambda}{\sqrt{\alpha\tau}\ \mathrm{erf}\left(\sqrt{t/\tau}\right) h_{conv}}\right)^{2.4}\right)^{\frac{1}{2.4}} h_{conv} \tag{23}$$

Besides, the value of n should logically depend on the fluid that is considered, and especially its Prandtl number Pr. In fact, the conductive and convective heat exchanges superposition is non-linear because the characteristic dimensions of heat exchange ways are different: convection is mainly due to the vorticity in the dynamic boundary layer and conduction works in the thermal boundary layer. The difference between thicknesses of both boundary layers is driven by the fluid Prandtl number. For instance, in a theoretical situation where both thicknesses would be identical ($Pr = 1$), the conduction and convection would overlap through the same layer and the parallel thermal resistances analogy could be used. Then, the global heat exchange coefficient could be calculated by a linear addition of conductive and convective heat exchange coefficients.

Hence, following this reasoning, if Pr is lower than 1, n should be lower than 1, and if Pr is greater than 1 (like for water), n should be greater than 1 too.

Other studies have been led in order to quantify transient heat exchanges between a wall heated up by an exponential heat source and different gases [25], with experiments similar to [19] and [18]. But, as these results are presented according to the power excursion period and not to the wall heat flux excursion period, which are quite different, and, as in these studies the material inertia is not negligible and should be taken into account, these results did not allow us to establish n for fluids with low Pr number. Furthermore, the range of excursion periods from those studies is too small to observe the asymptotic conduction in these experiments.

4 Analytical study of complete transient

4.1 Principles of the theoretical study

As already explained and presented in figure 2, the wall heat flux during a CABRI-RIA transient first presents an exponential increase and then remains quite constant. This section is thus dedicated to the evaluation of the total heat transfer coefficient during a complex reactivity insertion transient on CABRI. In fact, when external reactivity is inserted inside the CABRI reactor, the heat flux increases very fast during a first phase. This rise can be considered as being exponential. Then, this heat flux reaches a maximal value before it slowly decreases during a second phase. Rigorously, the heat exchange coefficient presented in eq. (23) cannot be used during the whole transient. This has been illustrated in fig. 7 where an example of heat flux computed by CATHARE2 (with a steady-state Dittus-Boelter heat exchange coefficient for illustration purpose) in a CABRI RIA transient is plotted (red plain line).

To simulate this kind of transient, it has been decided to complete the analytical heat transfer coefficient obtained in the previous phase. The associated theoretical simplified approach is drawn in red dash-line in fig. 7.

3 phases are considered in the simplified approach illustrated by the red dash-line in fig. 7:

- phase 0 is a steady-state; the heat exchange coefficient is given by a steady-state correlation.
- phase 1, beginning at t_1, is characterized by an exponential heat flux excursion; the heat exchange $h_{cond\ 1}$ is given by eq. (23).
- phase 2 is a transient phase where a wall maximal flux is reached. As the heat flux decreases very slowly (red plain line), a simplified approach will be made with the assumption of a constant heat flux.

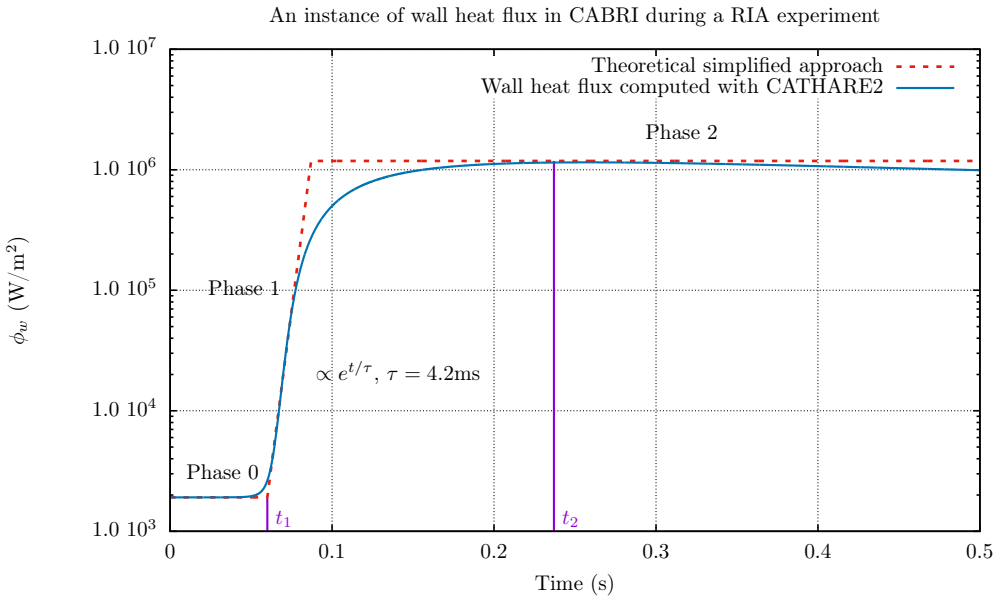

Figure 7: An illustration of the followed approach in the characterisation of heat exchanges during CABRI reactivity insertion transients

4.2 Determination of a heat exchange coefficient after the exponential excursion

Following the same methodology as in phase 1, we first derive the heat transfer coefficient in pure conduction corresponding to phase 2. Concerning this phase 2, the equations from eq. (4) to eq. (7) are still effective.
From now on, we write $\theta_2(x, t - t_2)$ as being the temperature difference $T(x, t > t_2) - T_\infty$ in the fluid during the phase 2.

The boundary condition is then :

$$-\lambda \frac{\partial \theta_2}{\partial x}\bigg|_0 = q_0'' e^{t_2/\tau} \tag{24}$$

Moreover, $\theta_2(x, 0)$ is nonzero number, which is related to the temperature profile that has been developed during the phase 1 in the fluid. Then, we have:

$$\theta_2(x,0) = \frac{q_0''}{\lambda}\frac{1}{2} e^{t_2/\tau}\sqrt{\alpha\tau}\left(e^{-x/\sqrt{\alpha\tau}}\mathrm{erfc}\left(\frac{x}{2\sqrt{\alpha t_2}} - \sqrt{\frac{t_2}{\tau}}\right) - e^{+x/\sqrt{\alpha\tau}}\mathrm{erfc}\left(\frac{x}{2\sqrt{\alpha t_2}} + \sqrt{\frac{t_2}{\tau}}\right)\right) \tag{25}$$

And considering the Laplace transform, it comes:

$$p\Theta_2 - \alpha\frac{\partial^2}{\partial x^2}\Theta_2 = \theta_2(x,0) \tag{26}$$

Finding particular solution of eq. (26) with $\theta_2(x, 0)$ defined in eq. (25) is not obvious. And the discrepancy between this asymptotic solution and the pure transitory solution is analytically demonstrated to be lower than 1% after 3τ. Moreover, the asymptotic regime is reached during the phase 1 in CABRI transient (*i.e.* $t_2 - t_1 > 3\tau$). Hence, in fig. 7 which figures out a CABRI transient simulated by CATHARE2, the transient duration under reactivity insertion lasts some tens of milliseconds, while the heat flux excursion period is $\tau \sim 4ms$. This enables to simplify the expression of $\theta_2(x, 0)$ and equation (26) becomes:

$$p\Theta_2 - \alpha\frac{\partial^2}{\partial x^2}\Theta_2 = \frac{q_0''}{\lambda} e^{t_2/\tau}\sqrt{\alpha\tau}\, e^{-x/\sqrt{\alpha\tau}} \tag{27}$$

The solution of this equation can be written as:

$$\Theta_2(x,p) = Ae^{-qx} + Be^{+qx} + \frac{q_0''}{\lambda} e^{t_2/\tau}\sqrt{\alpha\tau}\frac{1}{p - 1/\tau} e^{-x/\sqrt{\alpha\tau}} \tag{28}$$

As in phase 1, as the temperature is limited when $x \to +\infty$, then $B = 0$. By using the new boundary condition presented in eq. (24), we obtain after some steps:

$$\Theta_2(x,p) = \frac{q_0''}{\lambda} e^{t_2/\tau} \left(\left(\frac{-1}{q(p-1/\tau)} + \frac{1}{qp} \right) e^{-qx} + \sqrt{\alpha\tau} \frac{1}{p-1/\tau} e^{-x/\sqrt{\alpha\tau}} \right) \tag{29}$$

This can be inverted by using inverse Laplace transforms tables [24] and leads, for $t > t_2$ to:

$$\begin{aligned} \theta_2(x,t) =& \frac{q_0''}{\lambda} e^{t_2/\tau} \left[2\sqrt{\frac{\alpha(t-t_2)}{\pi}} e^{\frac{-x^2}{4\alpha(t-t_2)}} - x \ \mathrm{erfc}\left(\frac{x}{2\sqrt{\alpha(t-t_2)}} \right) \right] \\ & - \frac{q_0''}{\lambda} e^{t_2/\tau} \left[\frac{1}{2}\sqrt{\alpha\tau} e^{(t-t_2)/\tau} e^{-x/\sqrt{\alpha\tau}} \left(\mathrm{erfc}\left(\frac{x}{2\sqrt{\alpha(t-t_2)}} - \sqrt{\frac{(t-t_2)}{\tau}} \right) - 2 \right) \right] \\ & + \frac{q_0''}{\lambda} e^{t_2/\tau} \left[\frac{1}{2}\sqrt{\alpha\tau} e^{(t-t_2)/\tau} e^{+x/\sqrt{\alpha\tau}} \mathrm{erfc}\left(\frac{x}{2\sqrt{\alpha(t-t_2)}} + \sqrt{\frac{(t-t_2)}{\tau}} \right) \right] \end{aligned} \tag{30}$$

We deduce from this expression the theoretical conduction heat exchange, with the same method as in §3.1:

$$h_{cond\ 2}(t,\tau) = \frac{\lambda}{2\sqrt{\alpha(t-t_2)/\pi} + \sqrt{\alpha\tau} e^{(t-t_2)/\tau} \left(1 - \mathrm{erf}(\sqrt{(t-t_2)/\tau}) \right)} \tag{31}$$

The continuity of the conduction heat exchange coefficient is verified at t_2 under asymptotic assumption:

$$\lim_{t \to t_2^+} h_{cond\ 2}(t,\tau) = \frac{\lambda}{\sqrt{\alpha\tau}} = h_{cond\ 1}(t_2,\tau) \tag{32}$$

The total heat exchange coefficient can be deduced from the superposition of conduction and convection phenomena:

$$h_2(t,\tau) = \left(1 + \left(\frac{\lambda}{\left[2\sqrt{\alpha(t-t_2)/\pi} + \sqrt{\alpha\tau} e^{(t-t_2)/\tau} \left(1 - \mathrm{erf}(\sqrt{(t-t_2)/\tau}) \right) \right] h_{conv}} \right)^n \right)^{1/n} h_{conv} \tag{33}$$

In order to keep the continuity between h_1 (the total heat exchange coefficient in phase 1) and h_2 (the total heat exchange coefficient in phase 2) n must be taken equal to 2.4 ± 0.6 as in eq. (23).
In brief, the total heat exchange coefficient is:

$$h(t,\tau) = \begin{cases} h_{conv} & \text{if } t < t_1 \\ \left(1 + \left(\frac{\lambda}{\sqrt{\alpha\tau}\mathrm{erf}\left(\sqrt{(t-t_1)/\tau}\right) h_{conv}} \right)^{2.4} \right)^{\frac{1}{2.4}} h_{conv} & \text{if } t \in [t_1; t_2] \\ \left(1 + \left(\frac{\lambda}{\left[2\sqrt{\alpha(t-t_2)/\pi} + \sqrt{\alpha\tau} e^{(t-t_2)/\tau} \left(1 - \mathrm{erf}\left(\sqrt{(t-t_2)/\tau} \right) \right) \right] h_{conv}} \right)^{2.4} \right)^{\frac{1}{2.4}} h_{conv} & \text{if } t > t_2 \end{cases} \tag{34}$$

In order to illustrate this approach, the total heat exchange coefficient is drawn in fig. 8 for phases 1 and 2 (with $t_1 = 0$, $t_2 = 0.03$ s) for different heat flux excursion periods τ. The steady-state heat exchange coefficient (h_{conv} in black plain line) is determined for CABRI core with Dittus-Boelter standard correlation in CATHARE2. We can observe in this graph that the heat exchange coefficient reaches quite quickly its asymptotic value during the phase 1, in particular for small τ. This transient heat coefficient is far more significant than the steady-state value (in black). After the exponential excursion, at $t_2 = 0.03$ s, the heat exchange coefficient decreases and tends to its steady-state convection value. In this approach, the heat exchange coefficient is not differentiable at t_1 and t_2. This is due to the simplified approach presented in fig. 7 and leads to a slope break in the wall thermal heat exchange, that can not be avoided at this time. Moreover, the CABRI variation domain of τ is drawn on fig. 8 in order to give a hint of the transient heat exchange coefficient during CABRI transients. It appears that CABRI transients can be characterized by various excursion periods, that underlines the need to catch the clad-to-coolant heat transfer time dependence (*i.e.* before $t = 3\tau$).

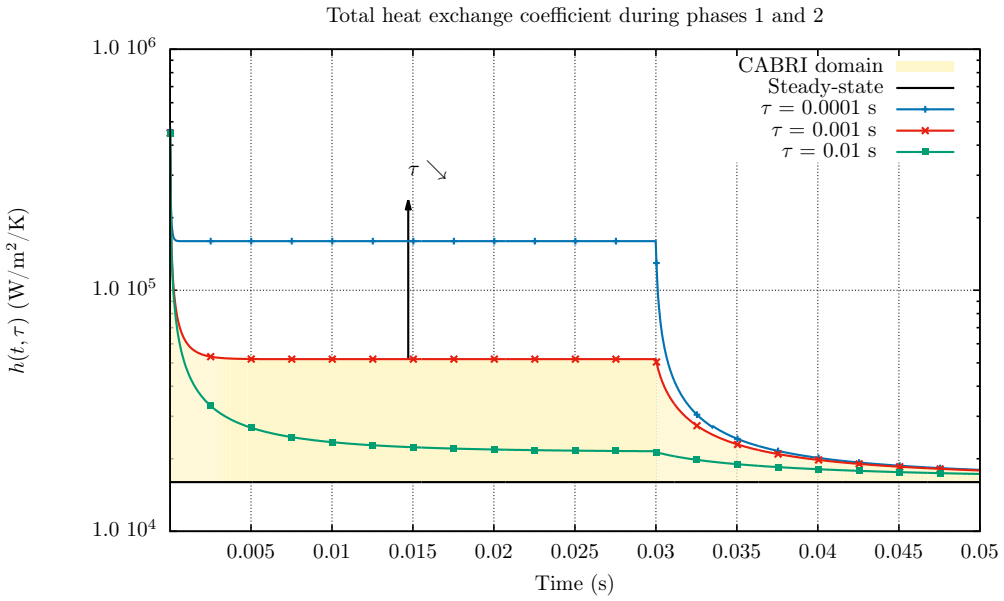

Figure 8: Total heat exchange coefficient during phases 1 and 2

5 CABRI thermal-hydraulics modeling with CATHARE2

5.1 Additional specifications on the geometry

This section focuses on the implementation of this total heat exchange coefficient (in eq. (34)) inside the CATHARE2 system code. The final goal of this work is to be able to simulate single-phase heat transfer under fast transient reactivity insertion in the CABRI core (heat flux excursion periods range between 10^{-3} s and 10^{-2} s) in the most predictive way. The CABRI core consists of several fuel rods assemblies which are different from the heated plate considered in MIT experiment [18]. The CABRI geometry being not a plane one, the heat exchange coefficient obtained with the analytical work presented in § 3.1 could be different if cylindrical geometry is considered. Actually, no analytical solution was found for the Laplace transform equation in cylindrical geometry. But assuming that the curvature effect is negligible in the boundary layer, results obtained in planar geometry remain valid. In order to justify this assumption, we calculate orders of magnitude of the Laplacian operator in heat conduction equation (cf. eq. (4)) for constant conductivity in cartesian and in cylindrical geometries:

$$\mathrm{div}(-\lambda\overrightarrow{\mathrm{grad}}(T)) = -\lambda\Delta T \tag{35}$$

Given that the characteristic dimension of the temperature variation δT is δ_t (thermal boundary layer thickness), the following orders of magnitude are deduced :

$$\begin{cases} \Delta_{car} T \sim \dfrac{\delta T}{\delta_t^2} & \text{(36a)} \\ \Delta_{cyl} T \sim \dfrac{1}{R}\dfrac{\delta T}{\delta_t} + \dfrac{\delta T}{\delta_t^2} & \text{(36b)} \end{cases}$$

Where R is the rods radius with $\delta_t \ll R$, so $\frac{\delta T}{\delta_t^2} \gg \frac{1}{R}\frac{\delta T}{\delta_t}$. In conclusion, the orders of magnitude of both cylindrical and cartesian Laplacians in the thermal boundary layer are similar. The transient heat conduction resolution in a plane geometry is representative of the one in a cylindrical geometry as long as the thermal boundary layer due to heat conduction remains much smaller than rods radius.

Moreover, the modeling takes into account axial variations of temperatures inside the rods (along z-axis), as it has not been considered in the previous analytical work (cf. fig. 3) and in experimental studies of [19]. So for the CATHARE2 meshing discretisation, the axial mesh height δz has been chosen in order to satisfy the next criterion:

$$\max\left(\frac{T_w(i+1) - T_w(i)}{\delta z}\right) \ll \frac{T_{w_{max}} - T_{w_{min}}}{z_{T_{max}} - z_{T_{min}}} \quad \forall i \tag{37}$$

Where i is the axial mesh index, $T_{w_{max}} = T_w(z_{T_{max}})$ is the maximal wall temperature. Satisfying this criterion, the wall temperature can be considered as constant on the height within each cell of the mesh. Thus its boundary condition is also constant. That makes the situation of fig. 3 consistent with a global extrapolation taking into account thermal axial profiles.

5.2 Steady-state heat exchange coefficient correlation

Given that the CABRI reactor core is subcooled, the default Dittus-Boelter steady-state correlation in the thermal-hydraulic tool CATHARE2 has been replaced by a Sieder-Tate correlation given that water flow in CABRI core is highly subcooled. This choice is consistent and has been validated during the experiments in [19]. The Sieder-Tate correlation is :

$$Nu_{ST} = 0.027 Re^{4/5} Pr^{1/3} \left(\frac{\eta_\infty}{\eta_w}\right)^{0.14} \tag{38}$$

It is similar to Dittus-Boelter correlation corrected by the ratio of water viscosities in the bulk (η_∞) and near the wall (η_w). The subcooling $T_\infty - T_{sat}$ is about 75 K in the CABRI core, and Re around 6 10^4. This correlation gives thus h_{conv} used in eq. (34).

5.3 Computation of heat exchanges excursion parameters

The implementation of the expression (34) in the CATHARE2 code implies the determination of three excursion parameters typical of each CABRI transient (displayed in figure 7): the time at the onset of the exponential heat flux excursion (t_1), the heat flux excursion period during phase 1 (τ) and the time when phase 1 ends and phase 2 starts.

Concerning t_1, it is obtained when the wall heat flux has increased of 20% from the initial wall heat flux in steady-state. It is thus determined in CATHARE2 as:

$$\phi_w(t_1) = 1.2\phi_w(t = 0) \tag{39}$$

With ϕ_w the wall heat flux. Studies show small sensitivity on the determination of t_1

The excursion period is obtained, given that the wall heat flux is considered as being exponential after t_1 (cf. fig. 7), solving this expression:

$$\frac{1}{\tau} = \frac{1}{\phi_w}\frac{\mathrm{d}\phi_w}{\mathrm{d}t} \tag{40}$$

As explained in the previous sections, the total heat exchange tends very quickly to a limit value during the exponential excursion phase. And, this limit value only depends on τ. As a consequence, the logarithmic derivative of the flux does not depend on the convective heat exchange in the eq. (40) and we simply implement in CATHARE2:

$$\frac{1}{\tau} = \frac{1}{T_w - T_\infty}\frac{\mathrm{d}(T_w - T_\infty)}{\mathrm{d}t} \tag{41}$$

The excursion period is then determined from the first ten simulation steps of the excursion with CATHARE2 in order to stabilise the calculation and to check that a converge value of this excursion period is obtained. This underlines the potential of this model whose parameters are based on code variables available over the calculation time. In that respect, only one multi-physics simulation is necessary to get the RI transient results (on the contrary to models which need the complete history of the power to calculate the heat flux evolution and thus require several calculations of the same transient to converge towards the solution).

Finally, t_2, which is the end of the exponential excursion, is derived in CATHARE2 as the time at which the wall temperature reaches a maximal value.

The analytical expression of the transient clad-to-coolant heat transfer (cf. eq. (34)) and these three excursion parameters have been implemented in CATHARE2. Next section presents some results of CABRI-RIA transients obtained with this new model in CATHARE2.

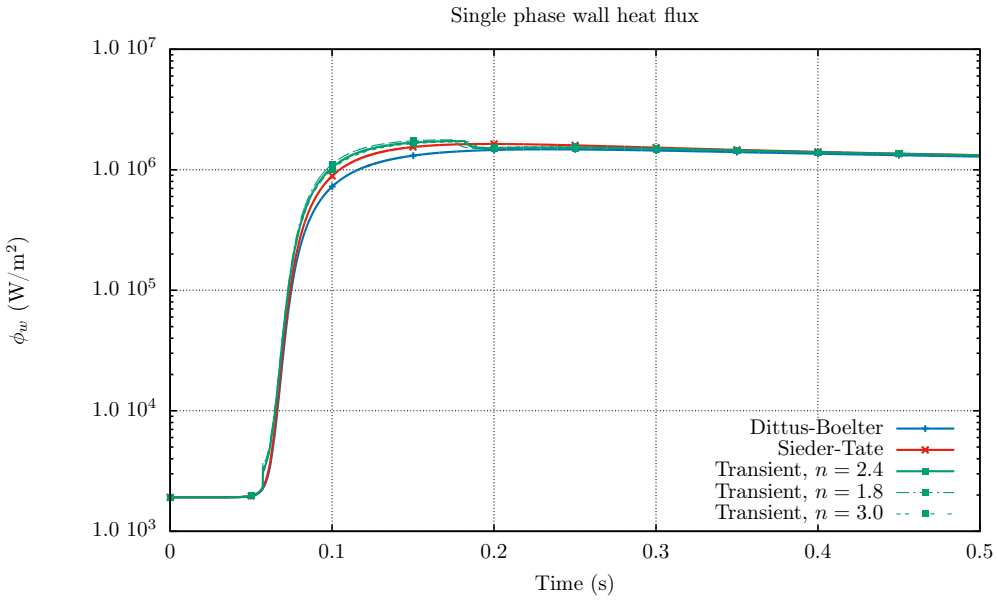

Figure 9: Effect on heat exchange coefficient model on single phase wall heat flux

5.4 Simulation of transient heat exchanges in the CABRI core

The aim of this section is to observe the impacts of using the new developed transient heat exchange correlation on some interest parameters of the CABRI core.The global validation of the CATHARE2 code version dedicated to RI transient (involving also neutronics and thermal-mechanical model improvement) is the purpose of the twin paper [6]. This section illustrates the variations of thermal-hydraulics variables in CATHARE2 under CABRI-RIA transients due to this new model.

The effect of the single-phase heat transfer modification has been studied on clad surface temperature, assembly outlet temperature and clad-to-coolant heat flux.
The chosen transient is representative of CABRI-RIA transients: a maximal instantaneous power of 16 GW and a Full Width at Half-Maximum of 9 ms. Further investigations on multiphysic interest parameters will be detailed in [6]. The energy is deposited into the pellet and the whole rod is modelled with the pellet-clad gap and the clad. The assembly is axially meshed and the results that are presented are taken at the bottom of the hottest sub-assembly. Rods are radially meshed too in accordance with the Biot number in a mesh respecting a criterion on the number of meshes N_{mesh}:

$$Bi_{mesh} = \frac{h_{conv} R / N_{mesh}}{\lambda_{fuel}} \ll 1 \tag{42}$$

With 20 radial meshes, we have $Bi_{mesh} \approx 8\ 10^{-4}$, satisfying this criterion.

Fig. 9 presents the wall heat flux computed with the two steady-state heat exchange correlations and this analytical transient expression (34) (where h_{conv} is given by the Sieder-Tate correlation). Dittus-Boelter being the default single-phase heat exchange correlation in CATHARE2, it is compared to the Sieder-Tate and the transient expression. One can see that the transient wall heat flux is higher during the exponential excursion than it is with steady-state correlations, but the difference is not really significant, given that the flux with transient heat exchange correlation stays in the range of 7 % of the one computed with Sieder-Tate correlation only. In this figure, two dropout behaviours could be noticed on the transient heat flux evolution around 0.065 s (t_1) and 0.2 s (t_2) resulting from the not differentiable features of the transient heat exchange coefficient around these two times.

However, the effect on the clad external temperature, presented in 10, is really noticeable. With the transient expression, the clad maximal temperature is reached after the wall heat flux excursion, and the maximal temperature discrepancy between transient correlation and Sieder-Tate correlation can reach 20 %. So the wall temperature discrepancy between the transient correlation and the Sieder-Tate correlation is similar to the the discrepancy between Dittus-Boelter correlation and Sieder-Tate correlation. In this figure, the discrepancy due to the uncertainty on n is also plotted. It has an impact on the maximal temperature during the wall heat flux excursion and on the

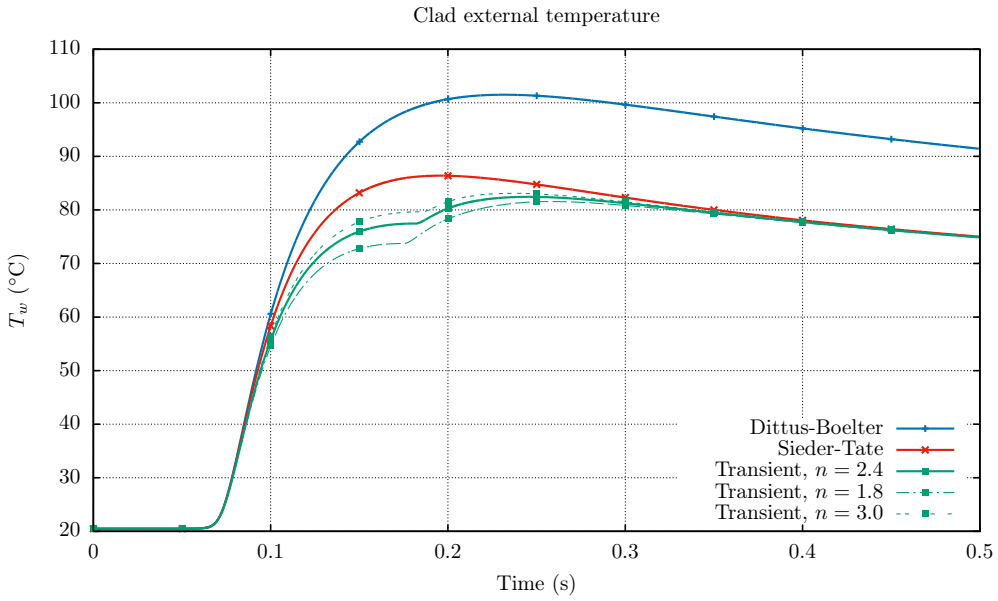

Figure 10: Effect on heat exchange coefficient model on clad temperature

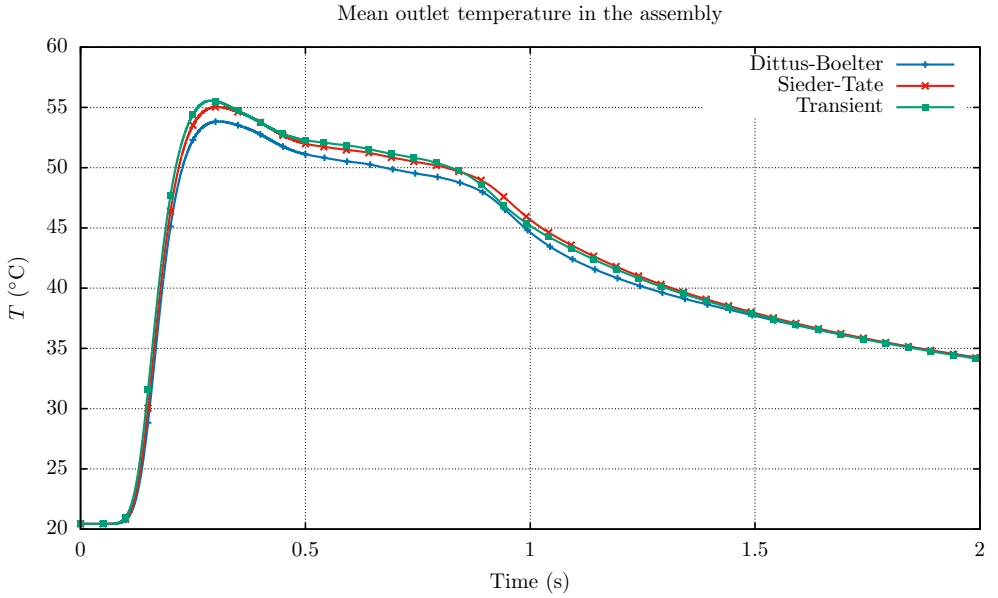

Figure 11: Effect on heat exchange coefficient model on outlet temperature

time when the temperature reaches a maximal value. The heat flux being more important in transient conditions, wall temperature are lower as displayed in 10. In the phase 2 (after $t > t_2 = 0.2$ s) the wall temperature normally converges to the steady-state value obtained in steady-state with the considered Sieder-Tate correlation. This is physically consistent. Finally, it is concluded that the effect of transient expression on clad temperature is already in single-phase not negligible during CABRI transients.

Fig. 11 then presents the assembly outlet temperature. The effect of transient expression on this parameter is less than 2 % in comparison with the steady-state Sieder-Tate correlation. This seems to suggest that the effect of transient single-phase heat transfer on global core outlet temperature will be really slight during CABRI transients.

Finally, even if the coefficient that has been developed for this transient situation gives consistent results in phase 1 (heat flux exponential excursion) and the following constant heat flux in phase 2, two slope breaks could be noticed in the wall heat flux and temperature between these phases (fig. 10 and 9). Their presence does not

prevent this model implementation and use in the CATHARE2 tool but it might still be improved. We tried to do numerically the same analytical work with a derivable function that could entirely describe (phase 1 and 2) the wall heat flux during the transient, for instance hyperbolic tangent function, or similar. But no analytical inverse Laplace transform of the temperature in the fluid with such complex boundary conditions has been found yet. The influence of the transient single-phase clad-to-coolant heat transfer seems to be limited during a CABRI-RIA transient on core thermal-hydraulics variables, except on local ones (wall temperature, wall heat flux). This model has been implemented in CATHARE2 with success. It will be the basement of the development in CATHARE2 of heat transfer coefficients for the successive boiling regimes in RI transient conditions. Once these models of boiling curve in transient conditions will be implemented in CATHARE2, we will pursue our experimental validation of this simulation tool on instrumented experiments dedicated to thermal-hydraulics phenomena, like for instance SPERT IV reactor where the main neutronic feedback effect limiting the power excursion is the void effect [26].

Conclusion and prospects

This analytical work is part of a broader effort leading to the improvement and validation of the multi-physics modeling of CABRI-RIA transients with the system tool CATHARE2. CATHARE2 is a highly verified and validated thermal-hydraulics system tool, which currently it is not adapted and thus validated for the simulation of very fast RIA transients such as CABRI transients. The final challenge is thus to succeed the simulation of the various multi-physics RI transients performed in the CABRI reactor catching the governing multiphysic phenomena with this CATHARE2 tool. After having reviewed the current capabilities of the CATHARE2 tool in regard to the main influential phenomena occurring during such RI transients, main improvements have been achieved [6] (in neutronics, thermal-mechanics...). In this context, the clad-to-coolant heat transfer has also been studied and the resulting work for single-phase flow is presented. This paper suggests a way to analytically model and quantify single-phase wall heat exchanges during reactivity insertion transients. It has been shown that in CABRI-RIA transients, the reactivity evolution is immediately limited by neutron feedback effects. Thus, the clad-to-coolant heat flux on one fuel rod of the CABRI core can be assimilated to an exponential heat flux during the early beginning of the transient but no longer after. Furthermore, the duration of this exponential wall heat flux excursion is very short in comparison to the duration of the whole RI transient. Therefore, expressions of the transient single-phase heat exchange coefficient derived by several authors in the literature is not applicable for a complete CABRI-RIA transient. Therefore, the proposed analytical expression for the clad-to-coolant heat exchange coefficient, improved from the studies of [18] and [20], could be implemented in a system code like CATHARE2 and simulate the whole CABRI-RIA transient and not only the first exponential part.

The first step of the work has led to the improvement of the clad-to-coolant heat exchange coefficient under an exponential heat flux (the very early phase of the RI transient). This coefficient is now a function of the time and of the excursion period. The second step has consisted in the establishment of a simplified approach in order to characterize the heat exchange coefficient during the whole RI transient, than can not rigorously be only taken equal to its value during the exponential excursion. Because the heat flux excursion is very short in comparison with the whole transient duration, the experimental studies performed with exponential power sources are not completely representative of RI transients.
The last step has aimed at implementing this model in CATHARE2, highlighting the potential of this model whose parameters are based on code variables available over the calculation time. Finally, the impact of this new correlation on complete and complex RI transients, performed in CABRI reactor, is observed. The transient that has been chosen is representative of CABRI tests and the influence of the transient heat exchange coefficient has been studied on three main local and global parameters: wall heat flux, clad external temperature and mean outlet temperature of the assembly.

Using the transient heat transfer coefficient correlation instead of a steady-state correlation increases the value of the calculated heat transfers and thus reduces the temperature peak reached at the clad surface. The effect of transient correlation on global parameters seems to be, in CABRI core, quite slight. This model has been implemented in CATHARE2 with success and will be the basement of the development of new correlations for the successive flow regimes in RIA transient conditions.

The validation step on separate effect tests of local thermal hydraulic behaviour will be quite difficult to be build with CABRI experiments, given that the only available experimental data are issued from very global measurements, with core inlet and outlet temperatures and mass flow-rate measurements. This validation step is tackled by the twin article [6].

Furthermore, the validation methodology of multiphysic calculation tools on the complex CABRI-RIA transients

established in [6], involving uncertainty propagation, will be achieved in order to quantify the effect of uncertainties on local and global thermal-hydraulic parameters in RI transients. Besides, the heat transfer coefficients derived for the successive boiling regimes in RI transient conditions might be validated on other instrumented experiments dedicated to boiling phenomena, like for instance SPERT IV reactor, where the main neutronic feedback effect limiting the power excursion is the void effect.

ACKNOWLEDGEMENTS

The authors would like to thank the IRSN, EDF and Framatome contributing to the study funding.

References

[1] G. Geffraye, O. Antoni, M. Farvacque, D. Kadri, G. Lavialle, B. Rameau, and A. Ruby. CATHARE 2 V2.5_2: A single version for various applications. *Nuclear Engineering and Design*, 241(11):4456–4463, November 2011.

[2] J-P. Hudelot, E. Fontanay, C. Molin, A. Moreau, L. Pantera, J. Lecerf, Y. Garnier, and B. Duc. CABRI facility: upgrade, refurbishment, recommissioning and experimental capacities. In *Proc. Int. Conf. PHYSOR2016*, Sun Valley, USA, 2016.

[3] J. Dugone. *SPERT III Reactor Facility: E-Core Revision*. IDO-17036 A EC Research and Development Report Reactor Technology TID-4500, Paris, 1965.

[4] P. Emonot and others. A new system code for thermal-hydraulics in the context of the NEPTUNE project. *Nuclear Engineering and Design*, 241(11):4476–4481, December 2011.

[5] Jean-Marc Labit. An advanced experimental validation methodology of multiphysics calculation tools on CABRI transients. In *Proceedings of M&C 2019*, volume 1, pages 2684–2695, Portland, Oregon, August 2019.

[6] J.-M. Labit, N. Marie, E. Merle, and O. Clamens. Multiphysics CATHARE2 modeling and validation of CABRI transients. *Nuclear Engineering and Design*, pages xx–xx, 2020.

[7] RELAP5/MOD3.2 code manual. Technical Report Report NUREG/CR-5535, US Nuclear Regulatory Commission, Washington DC, USA, 1995.

[8] H. Austregesilo and others. ATHLET models and methods. Technical Report Report GRS-P-1/Vol. 4, Gesellshaft fur Anlagen und Reaktorsicherheit, Garching, Germany, 2003.

[9] J. Staudenmeier. TRACE: TRACE/RELAP advanced computational engine 2004. In *Transactions of the 2004 nuclear safety research conference*, number NUREG/CP-0188, pages 25–27, oct 2004.

[10] V. Bessiron, T. Sugiyama, and T. Fuketa. Clad-to-Coolant Heat Transfer in NSRR Experiments. *Journal of Nuclear Science and Technology*, 44(5):723–732, May 2007.

[11] M. Suzuki and others. Analysis on pellet-clad mechanical interaction process of high burnup PWR fuel rods by RANNS code in reactivity-initiated accident conditions. *Nuclear Technology*, 155:282–292, 2006.

[12] T. Fuketa and others. Behavior of high-burnup PWR fuels with low-tin zircaloy-4 cladding under reactivity-initiated-accident conditions. *Nuclear Technology*, 133:50–62, 2001.

[13] T. Fuketa and others. A study of subcooled film-boiling heat transfer under reactivity-initiated accident conditions in light water reactors. *Nuclear Science and Engineering*, 88(3):331–341, 1984.

[14] K. Lassmann and others. Recent developments of the TRANSURANUS code with emphasis on high burnup phenomena. In *IAEA technical committee meeting on nuclear fuel behavior modeling at high burnup and its experimental support*, number IAEA-TECDOC-1233, pages 19–23, Windermere, UK, jun 2000.

[15] T. Sugiyama and others. Status of RIA related fuel safety research at JAEA. In *Fuel Behaviour and Modelling under Severe Transient and Loss of Coolant Accident (LOCA) Conditions*, number IAEA-TECDOC-CD-1709, pages 45–54, Mito, Japan, oct 2011.

[16] A. Arkoma. Extending the reactivity initiated accident (RIA) fuel performance code SCANAIR for boiling water reactor (BWR) applications. *Nuclear Engineering and Design*, 322:192–203, 2017.

[17] Reactivity initiated accident (RIA) fuel codes benchmark phase-II: Uncertainty and sensitivity analyses. Technical Report Report NEA/CSNI/R(2017)1, OECD Nuclear Energy Agency, Paris, France, 2017.

[18] G.-Y. Su, M. Bucci, T. McKrell, and J. Buongiorno. Transient boiling of water under exponentially escalating heat inputs. Part I: Pool boiling. *International Journal of Heat and Mass Transfer*, 96:667–684, May 2016.

[19] G.-Y. Su, M. Bucci, T. McKrell, and J. Buongiorno. Transient boiling of water under exponentially escalating heat inputs. Part II: Flow boiling. *International Journal of Heat and Mass Transfer*, 96:685–698, May 2016.

[20] A. Sakurai and M. Shiotsu. Transient Pool Boiling Heat Transfer—Part 1: Incipient Boiling Superheat. *Journal of Heat Transfer*, 99(4):547–553, November 1977.

[21] A. Sakurai, M. Shiotsu, K. Hata, and K. Fukuda. Photographic study on transitions from non-boiling and nucleate boiling regime to film boiling due to increasing heat inputs in liquid nitrogen and water. *Nuclear Engineering and Design*, 200(1):39–54, August 2000.

[22] A. Sakurai. Mechanisms of transitions to film boiling at CHFs in subcooled and pressurized liquids due to steady and increasing heat inputs. *Nuclear Engineering and Design*, 197(3):301–356, May 2000.

[23] M. W. Rosenthal. An Experimental Study of Transient Boiling. *Nuclear Science and Engineering*, May 1957.

[24] J. Hladik. *La transformation de Laplace à plusieurs variables*. Masson, 1969.

[25] Q. Liu, Z. Zhao, and K. Fukuda. Transient heat transfer for forced flow of helium gas along a horizontal plate with different widths. *International Journal of Heat and Mass Transfer*, 75:433–441, August 2014.

[26] S. Day. SPERT IV D-12/25: Facility specification. February 2015.